Molecular Dynamics Study on Glass Transitions in Atactic-Polypropylene Bulk and Freestanding Thin Films

Xiang Yu, Rongliang Wu, and Xiaozhen Yang*

Beijing National Laboratory for Molecular Sciences, Joint Laboratory of Polymer Science and Materials, State Key Laboratory of Polymer Physics and Chemistry, Institute of Chemistry, Chinese Academy of Sciences, Beijing 100190, China

Received: October 27, 2009; Revised Manuscript Received: March 10, 2010

Molecular dynamics simulation has been adopted in investigation of different glass transition behaviors of the bulk and the freestanding thin films (about 8 nm) of atactic polypropylene (*a*-PP). For characterization of glass transition temperature (T_g) of above systems, both the specific volume and the local conformational transition rate of the systems were examined. The T_g characterization from the local conformational transition rate of polymer chains was recently developed. Our simulation results show that the films have lower T_g than the bulk, and the descent of T_g is in a range of 30∼10 K. These are consistent with experiments. *a*-PP chain consists of meso-dyad and racemic-dyad, the above results are obtained from both dyads. Individual contribution of the stereoregular dyads to the conformational transition rate was further studied. It was revealed that T_g obtained singly from the meso-dyads was almost the same with T_g individually from the racemic-dyads, although the racemic-dyads have much lower transition rate and higher transition barrier than the meso-dyads. In the present study, the reason for the thin films having lower T_g than the bulk is attributed to the novel behavior that the films have lower transition rate and higher barrier than the bulk when it is below T_g. Such behavior was discussed according to the "coupling rotation" of the dihedrals, which depends on the increase of free volume and the inhibition of kinetic energy.

1. Introduction

The glass transition phenomenon in the thin polymer film was found different from that in the bulk. Many experimental techniques were employed to measure the glass transition temperature (T_g) in the thin or ultrathin films, for example, ellipsometry,[1−10] Brillouin light scattering,[11−13] photon correlation spectroscopy,[14] dielectric spectroscopy,[15−17] calorimetric measurements,[18−20] dynamics of fluorescent probes,[21] X-ray reflectivity[22−24] and so on. Many works had revealed that the T_g in the substrate supported film and the freestanding film is different from the bulk. Keddie et al[6] found that when the film was spin-casted on the substrate with which the interactions were supposed to be very weak, the T_g can decline about 20 K for the 10 nm thick films compared to the bulk. After that, numerous studies had also confirmed this effect.[1,3−5,7,8,11−17,21,25] On the contrary, when the film was strongly absorbed to the substrate, the T_g became obviously increased from that of the bulk.[1,7,9,21−23,26] For polymer freestanding thin films, in the past decade a number of researches[4,10,12,24,27,28] had revealed that T_g of the films were 30−70 K lower than that of the bulk. Original reason for the decrease or increase of T_g for the polymer film was studied in many efforts. For example, Kajiyama[25] thought the decrease of T_g was due to the increase of free volume near the surface region of thin films; Pham[7] pointed out that it was caused by the influence of confinement on the entropic contribution; Forrest et al[3,11,12] gave their explanation from the chain confinement effects or finite size effects depending on the M_n of the polymer chains. Ellison et al[21] reported the first experiment, in which they measured the T_g in the surface and the interior part of thin films. They found that the T_g in the surface part was 11−32 K lower than that in the interior part, and they thought the enhancement of dynamics at the surface affected T_g of regions several tens of nanometers into the film. In recent years, the percolation model for the glass transition phenomenon is of great interest to many researchers. Long and Merabia[29−31] theoretically studied the heterogeneous dynamics at the glass transition for the bulk and thin films and proposed a thermodynamical model. They argued that at T_g, termed the 3D glass transition temperature in their work, the slow domains no longer percolate for the freestanding films because of the quasi-2D nature of the film.

Although the experimental evidence has revealed probable aspects of the deviation of T_g in thin polymer film, direct observation on the microscopic molecular motion was not possibly obtained in these experiments. Studies with computer simulations give us the capability of gaining insight into microscopic details. One can find many studies[16,32−50] with computer simulation on the glass transition phenomena. Among all the computer simulation methods, molecular dynamics simulation is considered to be able to observe the dynamic motions at the atomistic level. Some studies[35,36,38,40] focused on the thermodynamic properties of the bulk system before and after the glass transitions. Some studies mainly focused on the local dynamics through the glass transition. Baljon et al[50] studied the glass transition of supported polymer film by molecular dynamics simulation. They analyzed the heterogeneous dynamics in the films and confirmed the percolation of immobile domains around the glass transition temperature. Takeuchi and Roe[32] studied the local chain dynamics around T_g using two polymer models. Later, Boyd and co-workers[33] studied the glass transition in bulk PE system using the conformational dynamics. They reported that the conformational transition rates remained Arrhenius through the glass transition and the disparity between the relaxation time and conformational transition behavior was

* To whom correspondence should be addressed.

10.1021/jp910245k
Published on Web 03/29/2010

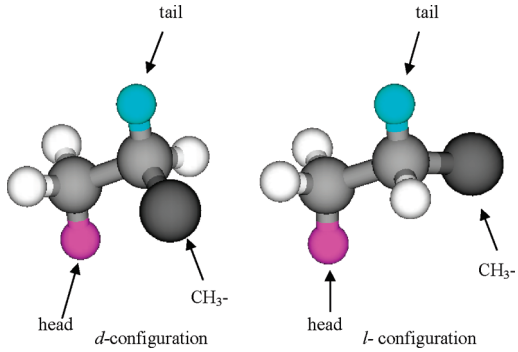

Figure 1. Two types of monomer that are used to built *a*-PP chains.

due to the increasingly heterogeneous of conformation jump as temperature decreased. Lyulin and Michels[42] simulated the glass transition of bulk atactic polystyrene in the vicinity of T_g, and the translational mobility was studied by measuring the mean-square translational displacement of monomers. It was found that the local translational mobility was separated into two diffusive regimes by a crossover regime describing the motions confined in cages formed by almost frozen neighborhood. Liang et al[39] studied the glass transition of single atactic polypropylene (*a*-PP) chain in NPT ensemble and found the "shallow jump" of dihedral was more responsible for the glass transition. Recently, Wu et al studied the conformational transition behaviors of polyethylene[51] (PE) and poly-(vinylidene fluoride)[52] (PVDF) around the glass transition temperature. In their works, the temperature dependence of conformational transition rate was found to have different Arrhenius behaviors above and below T_g. In other words, the conformational transition rate characterizes the glass transition well through the two different kinetic processes. They especially found that below T_g the conformational transition barrier was lower than that above T_g. They also found that the PE chain with higher M_n has a higher T_g and a lower transition barrier below T_g. To our knowledge, there is no computer research work on polymer thin film glass transition by tracing the conformational transition so far.

In the present study, we mainly focus on the conformational transition around T_g of *a*-PP bulk and freestanding thin film systems to show the difference between these two kinds of systems. The article was organized in the following sequence. In Section 2, the complex simulation details were described. In Section 3, first the T_g of the bulk and thin films were calculated by using the specific volume (or film thickness) and also the conformational transition rate. Then specific influence of meso- and racemic-dyads on conformational transition behaviors was discussed. At last, a probable physical explanation on the different transition behaviors between the bulk and the films were proposed.

2. Simulation Details

2.1. How to Create *a*-PP Chains. In the present work, *a*-PP chains were built by an OpenGL based computer simulation software, Virtual Molecules (VM), which was developed by our group. First, two types of monomers, the *d*-configuration and the *l*-configuration, were built as shown in Figure 1. In each monomer, one methyl group $-CH_3$ was treated as a united atom and other H− and C− atoms were treated as explicit atoms. The "head" atom and the "tail" atom labeled in the figure are for making a polymer chain from the monomers. When building the chain, the software connects such two monomers through aligning two bonds, the carbon−tail bond in the previous monomer and the carbon−head bond in the next monomer, and building a new C−C bond of 1.53 Å between the two monomers after eliminating the tail and head atoms. In this way a number of monomers were connected to create *a*-PP chain. There are four ways to generate a stereoregular dyad from the *d*- and *l*-configuration monomers, which are *dd*, *dl*, *ld*, *and ll*. Since experimentally *dl* and *ld* are not recognized from each other, the above stereoregular dyads are usually defined using the meso (*m*) and the racemic (*r*); the four stereoregular dyads become *m*, *r*, *r*, and *m*. To model the real *a*-PP chain system, we dealt with multiple chains in the system. We did not use many of the same chains with an atactic stereoregular sequence, but built each chain independently with different stereoregular sequences in the same atactic regularity ($m/r = 1:1$). The atactic regularity is a statistical average of two types of monomers randomly connected along the chain. In the use of Monte Carlo method to generate *a*-PP chains, we found that the longer chain length was generated the more accurate atactic regularity was obtained. But simulated chains are usually shorter (several tens of repeats), and it is thus difficult to generate a shorter chain with expected atactic regularity.

We introduced here an effective method of creating short chains with designed stereoregularity. It is to check the generation probabilities of *m* and *r*, or *mm*, *mr*, and *rr*, or *mmm*, *mmr*, *mrm*, *mrr*, *rmr*, and *rrr* for each short chain. The generated chain was chosen only when the chain having the least deviation of the probabilities in a run of 10^6 samplings. In this way, we made a number of *a*-PP systems ($m/r = 1:1$) with different chain lengths and different numbers of chains. After being built, each of the chains was forced to collapse into a globule by MD run under vacuum condition for 500 ps at 450 K.

2.2. How to Create the *a*-PP Bulk System and Ultrathin Freestanding Film Systems. In the present study, all the *a*-PP chains are in the same atactic regularity ($m/r = 1:1$). We mainly dealt with two *a*-PP systems, (1) the bulk system (90 repeat units per chain) and (2) a number of the ultrathin freestanding film systems with various thicknesses (90 repeat units per chain). We also created another bulk system with 22 repeat units in each chain. The last one was used as additional study in Section 3.4.

(i) The bulk system contains 8 different *a*-PP chains each consisting of 90 repeat units. Its simulation details were as follows:

Step 1. These eight globular chains were put in a cubic box with 3D periodic boundary condition (PBC), then the NPT MD simulations were carried out at 450 K for 20 ns with coupling to the external pressure of 1 atm. The autocorrelation function (ACF) of radius of gyration (R_g) and end-to-end vectors was traced and found to decline to zero within the simulation time, which means that the chains have interpenetrated each other. In this way, the bulk system at 450 K was created.

Step 2. The final structure of the MD trajectory at 450 K was picked out, and the temperature was quenched to 425 K to run another 20 ns MD. In the same way, the bulk systems at a series of temperatures (400, 375, 350, 325, 310, 300, 290, 280, 270, 250, 230, and 200 K) were created.

Step 3. The final structures of these bulk systems at each temperature were picked out and were used as initial structures for another 3 ns MD simulations at these temperatures respectively, without either optimization or reallocating atom speed. The trajectory files were saved every 0.1 ps, and the part after 500 ps in these trajectories were used for subsequent conformational transition analysis.

TABLE 1: Potential Functions and Parameters

	$V_{LJ}(\mathbf{r}_{ij}) = 4\varepsilon_{ij}((\sigma_{ij}/r_{ij})^{12} - (\sigma_{ij}/r_{ij})^{6})$	
	$\varepsilon_{ij} = (\varepsilon_{ii}\varepsilon_{jj})^{1/2}$	$\sigma_{ij} = (\sigma_{ii} + \sigma_{jj})/2$
nonbonded	ε_i (kJ/mol)	σ_i (nm)
C_3	0.397898	0.3473
C_33	1.046	0.284643
H_	0.063597	0.36994

	$V_b(r_{ij}) = \frac{1}{2}k_{ij}^b(r_{ij} - r_{ij}^0)^2$	
bonds	k_{ij}^b (kJ/mol/nm^2)	r_{ij}^0 (nm)
C_3-C_3	292880	0.153
C_3-H_	292880	0.109
C_3-C_33	292880	0.153

	$V_a(\theta_{ijk}) = \frac{1}{2}k_{ijk}^\theta(\theta_{ijk} - \theta_{ijk}^0)^2$	
bond angles	k_{ijk}^θ (kJ/mol/rad^2)	θ_{ijk}^0 (rad)
all angles	418.40	109.4710

	$V_d(\phi_{ijkl}) = k_\phi(1 + \cos(n\phi - \phi_0))$		
dihedrals	k_ϕ (kJ/mol)	ϕ_0 (rad)	n
X-C_3-C_3-X	0.464889	0	3

(ii) The freestanding film system contains the 48 chains with 90 repeat units. This system was created as follows:

Step 1. All the chains were put in a cubic 3D PBC box, and the NPT MD simulations were employed to make these chains interpenetrated with each other at 450 K and 1 atm. The interpenetration process was simulated for 20 ns, during which the ACF of average R_g and end-to-end vectors of these chains declined to 0, meaning the equilibrium of the interpenetration.

Step 2. The length in the *Z*-direction of the cubic box was enlarged to 20.0 nm, which made vacuum slabs above and below the interpenetrated *a*-PP chains. The lengths in the *X*- and *Y*-direction were changed from about 7.3 to 7.2 nm (using the "editconf" command in GROMACS tools), and then geometric optimization was performed to minimize the local energy. In this way, the lengths in the *X*- and *Y*-directions were shortened step by step until they got to the value of 7.0 nm.

Step 3. After the modification of box vectors, MD simulation was employed again. In this step, the NVT ensemble and 2D PBC with repeated images in *X*-, *Y*-directions were applied with the temperature set to 450 K. The MD simulation system got to the equilibrium state after 20 ns, and a piece of freestanding film was produced that stands for the *a*-PP film at 450 K. Then the final configuration was picked out and the temperature was quenched to 425 K to start MD simulation again for 20 ns, in this way another piece of *a*-PP film at 425 K was produced. Using the same procedure, the freestanding films at a series of temperatures (400, 375, 350, 325, 310, 300, 290, 280, 270, 250, 230, and 200 K) were created.

Step 4. After these freestanding films were created, they were used as initial structures for next MD simulations which were carried out again at these temperatures respectively without either optimizing their initial structures or reallocating atom speed. The trajectory files were saved every 0.1 ps and the total simulation time was 3 ns. The last 2.5 ns of the trajectories were used later for the analysis of glass transition.

Step 5. Using the same method in *Step* 2, other three freestanding thin film systems were created with *X*-, *Y*-lengths equal to 6.5, 7.5, and 8.0 nm, respectively. Then the same processes with *Steps* 3 and 4 were carried out at the same temperatures. All trajectory files took ~560 GB on the hard disk. The properties of the 4 film systems are listed in Table 2.

TABLE 2: The Situation of Four Thin Film Systems

films	*X*, *Y* PBC length/nm	thickness/nm (300 K)
film 1	6.5	8.8
film 2	7.0	7.6
film 3	7.5	6.6
film 4	8.0	5.8

(iii) The other bulk system contains 64 different short *a*-PP chains that consist of 22 repeat units. The simulation procedure is similar with that in (i). In the meantime, the conformational transition of a single short chain in the vacuum condition was simulated at these temperatures and its data will be compared with the bulk system.

2.3. The Software and Simulation Details. The OpenGL-based software Virtual Molecules was used to create all the *a*-PP chains. The open source software GROMACS 4.0[53] was used to run all the molecular mechanics (MM) optimization and molecular dynamics (MD) simulations, and the potential parameters from Dreiding II force-field[54] were used, as shown in Table 1. The cutoff for VdW potential was 0.9 nm. In the MD simulations, the time step for integration was 0.001 ps; Nose−Hoover temperature coupling algorithm was employed for all MD simulations and the Parrinello−Rahman pressure coupling method was applied for NPT ensembles. The time constant was 0.5 ps for temperature coupling and 4 ps for pressure coupling. The momentum correction was applied to reduce the displacement and rotation of mass center of the polymer chains in the periodic boundary and can also keep the chains in the center of the periodic boundary along *Z*-axis for the simulation of films in NVT ensembles.

3. Results and Discussion

3.1. T_g from the Specific Volume and the Film Thickness. According to the free volume theory, the specific volume varies linearly with temperature but has different slopes below and

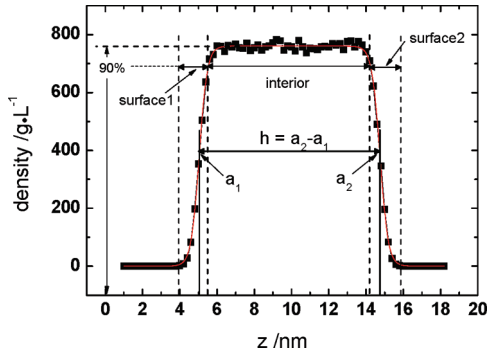

Figure 2. The density profile of *a*-PP thin film (Film 1, 450 K). The definition of thickness and the three parts of the film were labeled.

above the T_g. In many experiments, the T_g was measured by linearly fitting the specific volume curve at high and low temperature separately and finding the intersection of the two lines. Similar jobs were performed in T_g measurement for the thin film systems[1,7,9,13,23,55] by the relationship of thickness and temperature.

The measurement of thin film thickness was described in Figure 2. The similar measurement method was used by Xu[56] and originally developed by Helfand and Tagami,[57,58] and was slightly modified in the present study. After the density profile of the film was plotted in this figure, the first surface was fitted by eq 3.1 and the second surface was fitted by eq 3.2

$$y = \frac{1}{2}A_1\left(1 + \tanh\left(\frac{2(x - a_1)}{b_1}\right)\right) \tag{3.1}$$

$$y = \frac{1}{2}A_2\left(1 - \tanh\left(\frac{2(x - a_2)}{b_2}\right)\right) \tag{3.2}$$

Where A_1 and A_2 are the highest value of the density profile for each surface, and a_1 and a_2 are the half-width positions. After the a_2 and a_1 were obtained, the thickness of the thin film h was calculated as

$$h = a_2 - a_1 \tag{3.3}$$

Figure 3a illustrates the temperature dependence of specific volume for the bulk *a*-PP system. The intersection of the curves appears at 364 K, which stands for the T_g obtained in this MD simulation. However, the value from the MD simulation is much higher than the experimental value 253−262 K;[59,60] it was considered to be the consequence of the ultrahigh cooling rate (0.5 to 1 K/ns), which was much faster than that used in experiments and also the simpler stereoregularity situation than the experimental samples.[61] In the previous one-chain MD simulation,[39] the measured T_g of *a*-PP bulk was at 281 K, which was closer to the experimental value. The probable reason for the higher T_g obtained in the present multichain simulation than previous one-chain simulation was the longer relaxation time caused by entanglement for the multichain system, especially at low temperatures. Figure 3b shows the temperature dependence of thickness in *a*-PP freestanding thin film system. For the thickest film system (Film 1), the T_g appears at 358 K, that is 10 K lower than the bulk system. When the films got thinner, the T_g decreased as well. For Film 2, 3, and 4, the T_g's are 352, 338, 337 K, respectively. It should be noted that the films studied in experiments were usually from 10^2 nm to several tens of

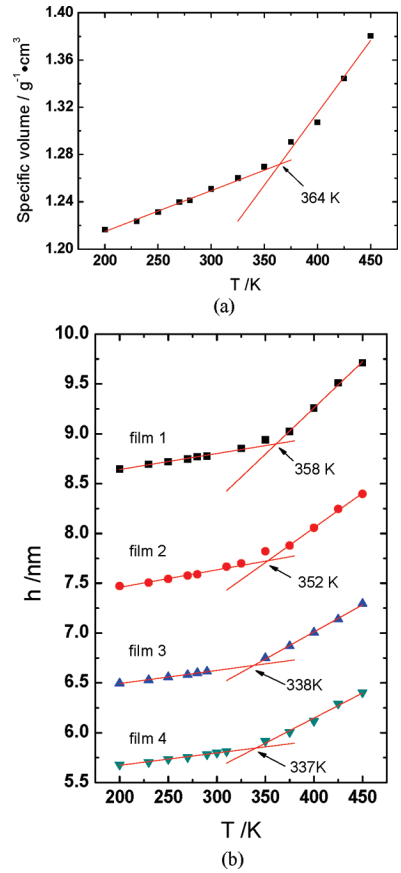

Figure 3. (a) The specific volume varies with temperature for bulk *a*-PP system. (b) The thickness varies with temperature for the 4 thin film *a*-PP systems.

nanometers in the thickness, which is much thicker than what we used (less than 10 nm) in the present simulation. But the trends of reduction of T_g with decreasing the film thickness in both experiments and present simulation are similar. The results show that the T_g's decrease about 10 to 30 K in thin films from that in bulk system. Our study thus gains the same scale of the descent of T_g obtained from above-mentioned experiments.[1,6−8,15,16,21]

3.2. T_g from Conformational Transition Rate. Measuring T_g by temperature dependence of specific volume or film thickness has proved the macroscopic rationality of the systems used in the present study. Further study would focus on the microscopic aspect when the glass transition takes place. There are several types of thermodynamic motions with different spatial scale that exist in the polymer system, among which the rotational isomeric state (RIS) transition that is also named as conformational transition is of local dynamics. The conformational transition of backbone is believed to be the very origin of the global changes in the polymer chain topology. Although some earlier works[32,33] found that there was no evident difference in the conformational transition behavior across the T_g, Wu's recent works[51,52] have proved the different Arrhenius behaviors of conformational transition rate above and below the T_g in different polymer systems. In the present work, the conformational transition behavior around the T_g was also traced in the bulk and ultrathin freestanding *a*-PP films with different thickness to investigate the glass transition of such *a*-PP systems.

The usual conformational transition rate[33] is defined as follows

$$k(i \rightarrow j) = \frac{N_{ij}}{\phi_i N t_s} \tag{3.4}$$

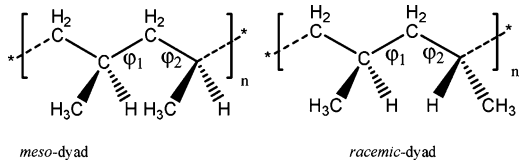

Figure 4. The meso- and racemic-dyads and the definition of φ_1 and φ_2.

where $k(i \rightarrow j)$ is the conformational transition rate of backbone bonds from RIS i to j, for example, from trans-conformation (t) to gauche-conformation (g); N_{ij} is the total number of such transition during the sample time t_s, N is the total number of backbone bonds in the system, ϕ_i is the fraction of backbone bonds in state i. This equation can be used for the polymer chains with single type of monomer, like PE and PVDF in previous works.[51,52]

But there is a structural feature that is the stereoregularity of the *a*-PP chain due to the existing chiral atoms in the chains and therefore the repeat units consist of meso- and racemic-dyads. Figure 4 shows the configurations of two stereodyads and a pair of involved bonds φ_1 and φ_2 as labeled in the figure. To calculate the conformational transition rate of *a*-PP chains, the φ_1 and φ_2 in each stereodyad should be traced separately. For such details, the specific conformational transition rate for φ_1, φ_2 in meso-dyad and in racemic-dyad cannot be calculated from eq 3.4. For clear explanation, we pick up the case with φ_1 and the meso-dyad in the definition below. The specific rate should be calculated from

$$k_{m1}(i \rightarrow j) = \frac{N_{ij,m1}}{\phi_{i,m1} N_{m1} t_s} \tag{3.5}$$

where $k_{m1}(i \rightarrow j)$ is the conformational transition rate for φ_1 of meso-dyad from state i to j. The subscript m means the meso-dyad (it can be r while in the case with racemic-dyad). The subscript 1 means φ_1. $N_{ij,m1}$ is the number of the specific transitions for φ_1 in meso-dyad, within the sample time t_s, N_{m1} is the total number of φ_1 in meso-dyad in the system, and $\phi_{i,m1}$ is the fraction of φ_1 in state i in meso-dyad.

In this way, the overall conformational transition rate k_m of φ_1 and φ_2 in meso-dyad is as follows, where $N_{ij,m} = N_{ij,m1} + N_{ij,m2}$, $N_m = N_{m1} + N_{m2}$ and $\phi_{i,m}$ is the overall fraction of φ_1 and φ_2 of meso-dyad in state i

$$k_m(i \rightarrow j) = \frac{N_{ij,m}}{\phi_{i,m} N_m t_s} \tag{3.6}$$

And

$$k_m = \frac{\sum_i \sum_j N_{ij,m}}{2 N_m t_s \sum_i \phi_{i,m}} \tag{3.7a}$$

Also, the conformational transition rate of bonds in racemic-dyads is

$$k_r = \frac{\sum_i \sum_j N_{ij,r}}{2 N_r t_s \sum_i \phi_{i,r}} \tag{3.7b}$$

Equations 3.7a and 3.7b will be used to calculate specific conformational transition rate in meso-dyads or in racemic-dyads in Section 3.2.2.

The overall conformation transition rate of the *a*-PP system is

$$k = \frac{\sum_i \sum_j (N_{ij,m} + N_{ij,r})}{2 t_s (N_m \sum_i \phi_{i,m} + N_r \sum_i \phi_{i,r})} \tag{3.8}$$

Now we have defined the various conformational transition rates of poly(α-olefin). Before calculating the rates, we have to determine RIS locations for each dihedral angle along *a*-PP chains. There are two types of conformational transitions found in our previous work,[51,52] the deep jump of dihedrals was defined as transition from one potential well (±10° from minimum) to another well (±10° from minimum) on the potential surface, and the shallow jump of dihedrals was defined as those from just jumping across the potential barrier top by 10° to any far within the RIS. To find out the RIS locations, the conformational potential was calculated from the equilibrated conformation distribution of the MD simulations.[26] Figure 5 shows the conformational potential energy curves in the equilibrated (450 K) *a*-PP bulk system. The curves for φ_1 and φ_2 in the meso- and racemic-dyads were plotted, respectively. In this figure, the deep jump is labeled as jumping from one region to another, where the two regions are both filled with diagonal lines, and the shallow jump is labeled as jumping from one region to another; both regions are filled with horizontal lines. Please note that the region of deep jump is included in the shallow jump as shown in the figure. We experienced that use of the deep jump alone will result in wrong barrier height with Arrhenius fitting. As the shallow jump was validated for obtaining correct measurement of the conformational transition barrier,[51,52] the shallow jump was adopted in calculating the conformational transition rate in the present work. As shown in the figure, the range of RIS was 10∼105° for the g^+ conformation, 125∼235° for the t conformation, and 255∼350° for the g^- conformation. Knowing the RIS regions of the shallow jump for each bond in the meso- and racemic-dyads, the calculation of eqs 3.5 to 3.8 can be carried out.

The conformational transition is a kinetic process. Barrier energy is significant for the process. The Arrhenius equation describes the relationship between the transition rate and the energy barrier

$$k = A \exp\left(-\frac{E_a}{RT}\right) \quad \text{or} \quad \ln k = -\frac{E_a}{R}\frac{1}{T} + \text{const} \tag{3.10}$$

Here E_a is the activity energy of conformational transition. The Arrhenius equation was used to measure the free energy barrier of shallow jump, just as in previous works.[33,51,52] The temperature dependence of overall conformational transition rate across the T_g of the bulk system and the thin film systems were

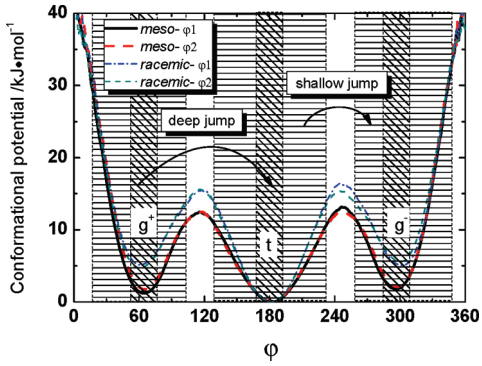

Figure 5. The conformational potential energy of φ_1, φ_2 in the meso- and racemic-dyads. The deep jump for the meso-dyads are labeled as jumping from one region to another, which are both filled with diagonal lines, and the shallow jump for the meso-dyads are labeled as jumping from one region to another, which are both filled with horizontal lines.

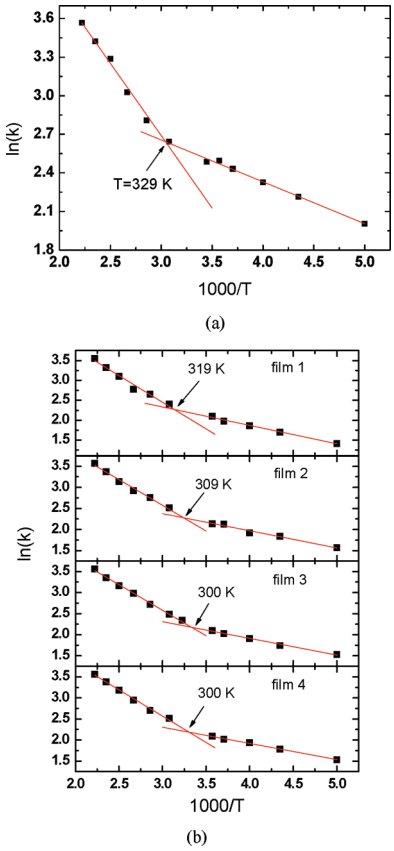

Figure 6. The temperature dependence of overall conformational transition rate for shallow jumps across T_g. (a) The bulk *a*-PP system. (b) The thin film *a*-PP systems.

given in Figure 6a,b respectively. Also, the overall T_g and transition barriers for all the systems are listed in Table 3a,b.

In Figure 6a, reversed temperature dependence of the logarithmic transition rate presents different behaviors at the high and the low temperature, and an intersection can be found at 329 K that regards the temperature of the glass transition for the bulk *a*-PP system. It was also found that the conformational transition barriers above T_g is higher than that below T_g. This phenomenon is the first novel behavior in the series studies of conformational transition characterization on the glass transition and is considered due to the "frozen" of RIS of bonds at low temperatures.[51,52] When the temperature was higher than T_g, the conformational transition rate along the *a*-PP chains were almost

TABLE 3

(a) The T_g Obtained from the Meso-, Racemic-, and the Overall Dyads in the Bulk and All the Thin Films (in K)

	overall	meso-	racemic-
bulk	329		
film 1	319	321	317
film 2	309	309	309
film 3	300	303	296
film 4	300	300	303

(b) The Conformational Transition Barrier for the Meso-, Racemic- and the Overall Dyads in the Bulk and All the Thin Films above and below T_g (in kJ/mol).

	overall	meso-	racemic-
above T_g			
bulk	9.35		
film 1	11.15	11.30	12.98
film 2	10.15	10.03	11.88
film 3	10.08	9.98	11.93
film 4	10.39	10.46	12.04
below T_g			
bulk	2.70		
film 1	3.84	3.90	4.14
film 2	3.38	3.63	3.36
film 3	3.29	3.05	4.45
film 4	3.22	3.17	3.79

homogeneous and only the bonds at the tails of the chain presented higher transition rate than that in the middle of the chain. But below T_g, the distribution of the conformational transition rates along the chain became much more heterogeneous. It can be found that the departure dihedrals of the shallow jumps were more closed to the barrier top. In this way, the conformational transition barrier becomes smaller. Such phenomena for PE and PVDF system had already been observed in our previous works.[51,52] In the present study, the same phenomenon for the *a*-PP systems was obtained. In Figure 6b, the film with the highest thickness (Film 1) has the highest T_g at about 319 K, which is 10 K lower than that of the bulk system. When the films become thinner, the corresponding T_g decrease as well from 319 to 309 and 300 K. The trend of the T_g decrease with thickness corresponds with many experiments.

The T_g observed by both ways, the specific volume and the conformational transition rate, were plotted in Figure 7. Obviously, both T_g data of decreasing with film thickness from the bulk are almost the same. The descent of T_g is about 10 to 30 K. Sakai et al[60] measured the T_g of the surface of *a*-PP thin film (251 K) and found it was 11 K lower than the T_g of the bulk (262 K), indicating the decreased T_g for the *a*-PP film from the bulk was about 10 K. The same decreasing value of T_g from

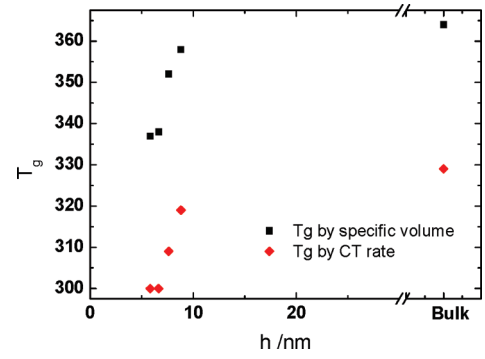

Figure 7. The T_g obtained by temperature dependence of specific volume (thickness) and the conformational transition rate.

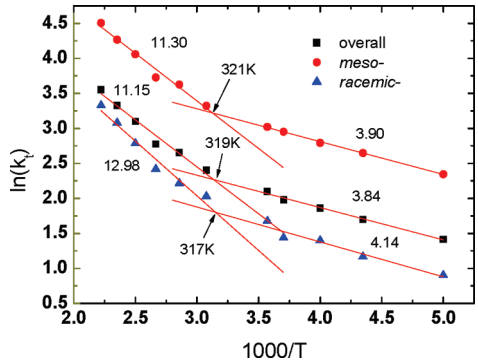

Figure 8. The temperature dependence of conformation transition rate for the meso-, racemic-, and the overall dyads in Film 1. The transition barriers are in kJ/mol.

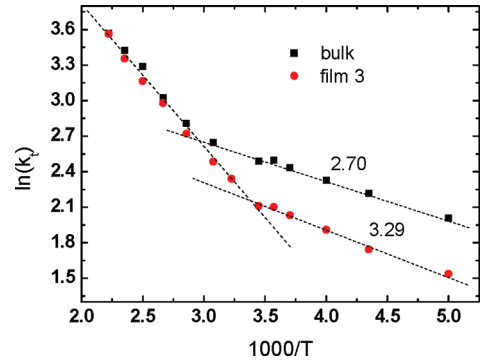

Figure 9. Comparison of overall conformational transition rate varies with temperature for the *a*-PP bulk system and one of the film systems (Film 3).

the bulk to the film was observed in present simulation, although the simulated T_g was higher than that in the experiments.

However, the T_g obtained by measuring conformational transition rate was about 40 K lower than those obtained by measuring the specific volume or thickness. The reason for this deviation was not exactly known but may be caused by different relaxation time of thermodynamic motions in the polymer system. The variation of specific volume or thickness was originated by the deformation and movement of entire polymer chains, whose relaxation time was much longer than conformational transition process. In the MD simulation, the ultrahigh quenching rate made the chains uncompleted relaxed, especially at low temperatures, which then resulted in the higher T_g as measured. The conformational transition from one RIS to another would be complete in less than several tens of picoseconds, thus the transition rate might not be influenced seriously by the ultrahigh quenching rate. Therefore, the T_g obtained by the $\ln(k) \sim 1/T$ relationship was found to be very close to the experiment values.

3.3. Different Conformation Transition Behaviors of Meso- and Racemic-Dyads. As the *a*-PP chains have meso- and racemic-dyads randomly linked along the chains. In this section, influence of the two stereodyads to the conformational transition behavior will be discussed. The conformational transition rates of chemical bonds in meso- and racemic-dyads in the films were calculated according to eq 3.7a and 3.7b proposed in Section 3.2.

Figure 8 shows the $\ln(k) \sim 1/T$ relationship for the meso-, racemic- and overall dyads of Film 1. The following can be found. (i) The conformational transition rate of meso-dyads was much faster than the racemic-dyads. (ii) The T_g obtained by finding the intersection of the fitting lines was 321 K for meso-dyads, 317 K for racemic-dyads, and 319 K for overall. It shows a 4 K difference between the meso and the racemic. The differences for Film 2, 3, and 4 listed in Table 3a are 0, 7, and −3 K, respectively. Averaging the four films, the difference is 2 K. (iii) In both temperature ranges, above and below T_g, the conformational transition in racemic-dyads has the higher barrier than that in meso-dyads. The result was supported by the potential curves calculated from RIS population distribution in the present MD simulation as shown in Figure 5. Obviously in this figure the potential energy between the well bottom of *t* and the peak top of $t \rightarrow g$ transition were different for meso- and racemic-dyads, and the racemic-dyads have the higher potential difference than the meso-dyads, corresponding with the conformational transition barrier data. The other three thin films showed the same trend (Table 3).

Ellison et al[21] proposed that the T_g of the surface part in polymer films was lower than the interior part. In the present work, we tried to divide the films into surface and interior parts (Figure 2) and calculate the T_g of each part. But it was found that the T_g were almost the same values for the surface and interior parts in all the films, indicating the films used here (8.8−5.8 nm) were too thin to be separated. This is supported by experimental results that indicating the thickness of the surface layer is about 10 nm.[21]

3.4. Different Conformational Transition Behaviors of the Bulk and the Films. The T_g of the freestanding ultrathin film systems was found lower than that of the bulk system in the present simulation, which is consistent with experimental observations. The simulated results thus provide a chance to gain the insight into atomistic level in the bulk and the films. Below, we will show second novel behavior, which was found in characterization of the glass transition through the window of conformational transitions of main chain backbone of polymers.

Figure 9 shows the curves of $\ln(k)$ vs $1/T$ for the bulk and Film 3. At high temperatures, the conformational transition rates of both systems appear in almost the same fitting curve. This means that the transition rate and the transition barrier at high temperatures were nearly the same. Below T_g, we found that the curve for the bulk turns to a smaller slope before that for the film does. Surprisingly, at a temperature of the glass state the conformational transition rate in the bulk is always higher than that in the film. Since the film has more free rooms than the bulk, the film should generally be speculated to have the higher transition rate, but the simulation shows the different case. This is the second novel behavior we found in our resent studies. In our earlier works,[51,52] we found in characterization of the glass transition by using the conformational transition rate, the barrier height of the transition behavior for the glass state is lower than that for the liquid state. This is the first novel behavior. And Figure 9 shows the second novel behavior. The mechanism of the first novel behavior was attributed to the departure dihedrals of rotors moving close to the top of the barrier and the transition dihedrals turning to sweeping smaller angles.[51,52] Mechanism of the second novel behavior will be discussed in this section.

Below T_g, we also found another feature that the barrier of the conformational transition in the bulk (2.70 kJ/mol) was lower than that in the film (3.29 kJ/mol). All the data of T_g and the barrier height for the bulk and the four films are listed in Table 3a,b, showing the same features.

The physical reason for the lower conformational transition rate and the higher barrier in the *a*-PP freestanding thin films below T_g was considered here to be influenced by the surfaces. Ordinarily, the surface in the films is thought to possess more

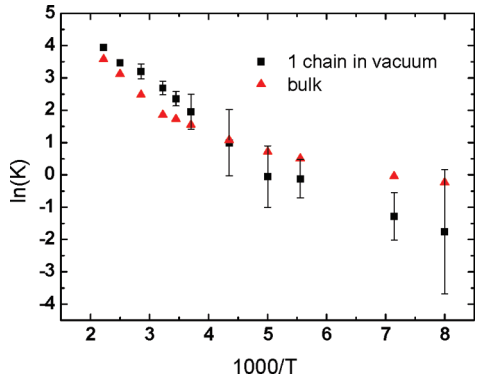

Figure 10. Temperature dependence of conformational transition rate of the *a*-PP bulk (22 repeat units chains) and single chain in vacuum condition.

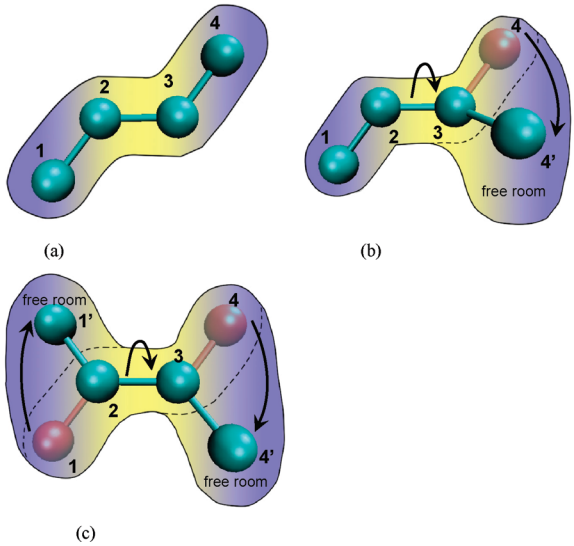

Figure 11. (a) Frozen bond in trans-state; (b) conformational transition of a bond from trans- to gauch-state with one free room; (c) coupling rotation of two dihedrals with two free rooms.

free volume and the dihedral bonds are more likely to rotate. The surface is thus considered an introduction of more conformational transitions. But actually, the surface not only increases the conformational transitions but can also decrease the conformational transitions at low temperatures.

To get better understanding, we simulated another two systems. One is a 22 repeat unit *a*-PP chain with other 63 the same length *a*-PP chains in the bulk environment. The other is such a *a*-PP chain in the vacuum. We used short chain here to avoid forming globule in the single chain under the vacuum condition. Generally, one may speculate that the chain in the vacuum should have higher transition rate than that in the bulk. Figure 10 shows results of the simulations where at higher temperatures the single chain in the vacuum condition has higher conformational transition rate. But the situation is reversed at low temperatures where the bulk has higher conformational transition rate. This phenomenon is similar with the situation between the bulk and the films below T_g as shown in Figure 9.

The novel behavior found in the present study must have unusual mechanism. A probable physical reason for this phenomenon was proposed here as the "coupling rotation" of the dihedral bonds. Figure 11a shows a model in trans-conformation, it concerns three chemical bonds with four backbone atoms, and the conformational transition will occur to the bond connecting Atom 2 and Atom 3. The transition cannot occur to the case without free room for Atom 1 or Atom 4. When the Atom 4 has a free room as shown in Figure 11b, the model has a chance to transit from the trans-conformation to the gauche-conformation. This shows that the more free room the system has, the higher transition rate the system possesses. However when the model has two more free rooms (Figure 11c), that is, Atom 4 can rotate to Atom 4′ and Atom 1 can also move to Atom 1′, the conformational transition may end in failure. This is because before Atom 4 reaches the place of Atom 4′, Atom 1 can move to Atom 1′. In other words, there is a coupling between Atom 4 rotation and Atom 1 rotation, consequently the trans-conformation undergoes a failed transition without crossing the top to the gauche-conformation but remains still in the trans-conformation. This can be more likely to happen at low temperatures as the atoms have lower kinetic energies.

On the whole, the more free rooms the coupling rotation can have, the more coupling rotation can make the conformational transition broke down. Obtained results show that the coupling rotation happens at low temperature, especially for the system having more free rooms. The same physical prospect can be considered in explanation of the *a*-PP freestanding thin films having lower transition rate and higher barrier height than that of the bulk.

4. Conclusion

Different glass transition behaviors of the bulk and the ultrathin freestanding film of *a*-PP systems have been studied by using MD in the present work. The *a*-PP chains were built by an effective method, which resulted in the short chains with the designed atactic regularity ($m/r = 1:1$). Simulated results show that the T_g of the thin films decrease about 10 to 30 K from the T_g in the bulk. The present study thus gains the same scale of the descent of T_g as obtained from experiments.[1,6−8,15,16,21] The decreasing curves of T_g versus temperature obtained from both the specific volumes and the conformational transition rates appear similarly. It manifests that the recently developed characterization of the conformational transition behavior on the glass transition[39,51,52] efficiently relates the macroscopic properties to the local dynamics.

Conformational transition behavior occurs to *a*-PP chains in the meso- and racemic-dyads. We analyzed the behavior in terms of either one of the two stereodyads. It was found that T_g individually calculated from either the dyads are nearly the same, and that the meso-dyad has much faster conformational transition rate and lower transition barrier than that of the racemic-dyad.

When the conformational transition rate and the barrier height between the bulk and the films were compared, we found a novel behavior that the films have much lower transition rate and higher transition barriers than the bulk below T_g. Existence of this behavior was further validated with two more system simulations. The physical reason is considered here to be concerned with the coupling rotation of the dihedral bonds, which is likely to occur at low temperatures with limited kinetic energy, and the coupling rotation makes the conformational transition broken down. In this way, the thin film has lower T_g than the bulk. The present study indicates that the phenomenon of the film having the lower T_g than the bulk is attributed to both the increase of free volume and the limitation of kinetic energy.

Acknowledgment. We acknowledge the support from National Science Foundation of China (20874107).

References and Notes

(1) Park, C. H.; Kim, J. H.; Ree, M.; Sohn, B. H.; Jung, J. C.; Zin, W. C. *Polymer* **2004**, *45*, 4507.
(2) Dalnoki-Veress, K.; Nickel, B. G.; Roth, C.; Dutcher, J. R. *Phys. Rev. E* **1999**, *59*, 2153.
(3) Forrest, J. A.; Mattsson, J. *Phys. Rev. E* **2000**, *61*, R53.
(4) Mattsson, J.; Forrest, J. A.; Borjesson, L. *Phys. Rev. E* **2000**, *62*, 5187.
(5) Kawana, S.; Jones, R. A. L. *Phys. Rev. E* **2001**, *6302*, 021501.
(6) Keddie, J. L.; Jones, R. A. L.; Cory, R. A. *Europhys. Lett.* **1994**, *27*, 59.
(7) Pham, J. Q.; Green, P. F. *J. Chem. Phys.* **2002**, *116*, 5801.
(8) Pham, J. Q.; Green, P. F. *Macromolecules* **2003**, *36*, 1665.
(9) Grohens, Y.; Brogly, M.; Labbe, C.; David, M. O.; Schultz, J. *Langmuir* **1998**, *14*, 2929.
(10) Herminghaus, S.; Jacobs, K.; Seemann, R. *Eur. Phys. J. E* **2001**, *5*, 531.
(11) Forrest, J. A.; DalnokiVeress, K.; Stevens, J. R.; Dutcher, J. R. *Phys. Rev. Lett.* **1996**, *77*, 2002.
(12) Forrest, J. A.; DalnokiVeress, K.; Dutcher, J. R. *Phys. Rev. E* **1997**, *56*, 5705.
(13) Dalnoki-Veress, K.; Forrest, J. A.; Murray, C.; Gigault, C.; Dutcher, J. R. *Phys. Rev. E* **2001**, *6303*, 031801.
(14) Forrest, J. A.; Svanberg, C.; Revesz, K.; Rodahl, M.; Torell, L. M.; Kasemo, B. *Phys. Rev. E* **1998**, *58*, R1226.
(15) Fukao, K.; Miyamoto, Y. *Phys. Rev. E* **2000**, *61*, 1743.
(16) Hartmann, L.; Gorbatschow, W.; Hauwede, J.; Kremer, F. *Eur. Phys. J. E* **2002**, *8*, 145.
(17) Sharp, J. S.; Forrest, J. A. *Phys. Rev. E* **2003**, *67*, 031805.
(18) Fryer, D. S.; Nealey, P. F.; de Pablo, J. J. *Macromolecules* **2000**, *33*, 6439.
(19) Fryer, D. S.; Peters, R. D.; Kim, E. J.; Tomaszewski, J. E.; de Pablo, J. J.; Nealey, P. F.; White, C. C.; Wu, W. L. *Macromolecules* **2001**, *34*, 5627.
(20) Efremov, M. Y.; Warren, J. T.; Olson, E. A.; Zhang, M.; Kwan, A. T.; Allen, L. H. *Macromolecules* **2002**, *35*, 1481.
(21) Ellison, C. J.; Torkelson, J. M. *Nat. Mater.* **2003**, *2*, 695.
(22) vanZanten, J. H.; Wallace, W. E.; Wu, W. L. *Phys. Rev. E* **1996**, *53*, R2053.
(23) Wallace, W. E.; Vanzanten, J. H.; Wu, W. L. *Phys. Rev. E* **1995**, *52*, R3329.
(24) Miyazaki, T.; Inoue, R.; Nishida, K.; Kanaya, T. *Eur. Phys. J.* **2007**, *141*, 203.
(25) Kajiyama, T.; Tanaka, K.; Takahara, A. *Polymer* **1998**, *39*, 4665.
(26) Carriere, P.; Grohens, Y.; Spevacek, J.; Schultz, J. *Langmuir* **2000**, *16*, 5051.
(27) Guerin, G.; PruD'Homme, R. E. *J. Polym. Sci., Part B: Polm. Phys.* **2007**, *45*, 10.
(28) Rotella, C.; Napolitano, S.; Wubbenhorst, M. *Macromolecules* **2009**, *42*, 1415.
(29) Long, D.; Lequeux, F. *Eur. Phys. J. E* **2001**, *4*, 371.
(30) Merabia, S.; Long, D. *Eur. Phys. J. E* **2002**, *9*, 195.
(31) Merabia, S.; Sotta, P.; Long, D. *Eur. Phys. J. E* **2004**, *15*, 189.
(32) Takeuchi, H.; Roe, R. J. *J. Chem. Phys.* **1991**, *94*, 7458.
(33) Boyd, R. H.; Gee, R. H.; Han, J.; Jin, Y. *J. Chem. Phys.* **1994**, *101*, 788.
(34) Han, J.; Boyd, R. H. *Macromolecules* **1994**, *27*, 5365.
(35) Yu, K. Q.; Li, Z. S.; Sun, J. Z. *Macromol. Theor. Simul.* **2001**, *10*, 624.
(36) Yang, L.; Srolovitz, D. J.; Yee, A. F. *J. Chem. Phys.* **1999**, *110*, 7058.
(37) Fukuda, M.; Kikuchi, H. *J. Chem. Phys.* **2000**, *113*, 4433.
(38) Rigby, D.; Roe, R. J. *J. Chem. Phys.* **1987**, *87*, 7285.
(39) Liang, T. N.; Yang, Y.; Guo, D. W.; Yang, X. Z. *J. Chem. Phys.* **2000**, *112*, 2016.
(40) Pozuelo, J.; Baselga, J. *Polymer* **2002**, *43*, 6049.
(41) Negi, A.; Basu, S. *Modell. Simul. Mater. Sci. Eng.* **2006**, *14*, 563.
(42) Lyulin, A. V.; Michels, M. A. J. *Macromolecules* **2002**, *35*, 1463.
(43) Canales, M.; Sese, G. *J. Mol. Liq.* **2007**, *136*, 206.
(44) Buchholz, J.; Paul, W.; Varnik, F.; Binder, K. *J. Chem. Phys.* **2002**, *117*, 7364.
(45) Santen, L.; Krauth, W. *Nature* **2000**, *405*, 550.
(46) Mischler, C.; Baschnagel, J.; Binder, K. *Adv. Colloid Inter.* **2001**, *94*, 197.
(47) Varnik, F.; Baschnagel, J.; Binder, K.; Mareschal, M. *Eur. Phys. J. E* **2003**, *12*, 167.
(48) Scheidler, P.; Kob, W.; Binder, K. *Europhys. Lett.* **2002**, *59*, 701.
(49) Scheidler, P.; Kob, W.; Binder, K. *J. Phys. Chem. B* **2004**, *108*, 6673.
(50) Baljon, A. R. C.; Billen, J.; Khare, R. *Phys. Rev. Lett.* **2004**, *93*, 255701.
(51) Wu, R. L.; Zhang, X. F.; Ji, Q.; Kong, B.; Yang, X. Z. *J. Phys. Chem. B* **2009**, *113*, 9077.
(52) Wu, R. L.; Kong, B.; Yang, X. Z. *Polymer* **2009**, *50*, 3396.
(53) Hess, B.; Kutzner, C.; van der Spoel, D.; Lindahl, E. *J. Chem. Theory. Comput.* **2008**, *4*, 435.
(54) Mayo, S. L.; Olafson, B. D.; Goddard, W. A., III *J. Phys. Chem.* **1990**, *94*, 8897.
(55) Singh, L.; Ludovice, P. J.; Henderson, C. L. *Thin Solid Films* **2004**, *449*, 231.
(56) Xu, G. Q.; Mattice, W. L. *J. Chem. Phys.* **2003**, *118*, 5241.
(57) Helfand, E.; Tagami, Y. *J. Chem. Phys.* **1972**, *57*, 1812.
(58) Helfand, E.; Tagami, Y. *J. Chem. Phys.* **1972**, *56*, 3592.
(59) Kaufmann, H. S.; Falcetta, J. J. *Introduction to Polymer Science and Technology*; Wiley: New York, 1977.
(60) Sakai, A.; Tanaka, K.; Kajiyama, T.; Takahara, A. *Polymer* **2002**, *43*, 5109.
(61) Zhu, S.; Yang, X.; Chujo, R. *Polym. J.* **1983**, *15*, 859.

JP910245K